METALLURGY

Cryoforged nanotwinned titanium with ultrahigh strength and ductility

Shiteng Zhao[1,2,3]*†, Ruopeng Zhang[1,2]†, Qin Yu[4], Jon Ell[1,4], Robert O. Ritchie[1,4], Andrew M. Minor[1,2]*

Nanostructured metals are usually strong because the ultrahigh density of internal boundaries restricts the mean free path of dislocations. Usually, they are also more brittle because of their diminished work-hardening ability. Nanotwinned materials, with coherent interfaces of mirror symmetry, can overcome this inherent trade-off. We show a bulk nanostructuring method that produces a multiscale, hierarchical twin architecture in a hexagonal closed-packed, solute-free, and coarse-grained titanium (Ti), with a substantial enhancement of tensile strength and ductility. Pure Ti achieved an ultimate tensile strength of almost 2 gigapascals and a true failure strain close to 100% at 77 kelvin. The multiscale twin structures are thermally stable up to 873 kelvin, which is above the critical temperature for many applications in extreme environments. Our results demonstrate a practical route to achieve attractive mechanical properties in Ti without involving exotic and often expensive alloying elements.

Titanium (Ti) has the highest strength-to-weight ratio among all the metallic elements, which, in addition to its outstanding corrosion resistance, renders it ideal for a variety of weight- and environment-sensitive load-bearing applications (*1*). The strength of pure Ti, however, is moderate. One way to harden Ti is to alloy it with other elements such as oxygen (O), aluminum (Al), and vanadium (V), forming either a solid solution or secondary phases (*1*). The strength of these alloys is improved, but almost always at the expense of the ductility.

An alternative route to strengthening structural metals is by tailoring the grain size through thermal-mechanical processing (*2*, *3*). Specifically, reducing grain size to a submicrometer and nanometer regime leads to a substantial increase in the yield strength (*4*–*6*), whereas ductility can be preserved when certain types of interfaces are introduced (*7*, *8*). In this respect, the past two decades has witnessed the successful development of nanotwinned metals. Numerous studies in face-centered cubic (fcc) metals suggest that twinning can lead to a much-improved strength without sacrificing resistance to fracture (*9*, *10*). This observation is attributed to the coherent nature of the twin boundary, which can both block and transmit incoming dislocations, depending on their characteristics, and thus provide strength and ductility, respectively (*11*). By tailoring the spacing and orientation of twin lamellae, the mechanical properties can be optimized even further (*8*, *12*, *13*). Nanotwinned copper with a gradient microstructure exhibits enhanced strength because of an extra work-hardening capacity (*14*), whereas highly oriented nanotwinned copper displayed an enhanced fatigue resistance because of the distinct dislocation pathways (*15*). Twin boundaries also represent low-energy boundaries with a much-reduced mobility at elevated temperatures. This property renders them thermally more stable than random high-angle grain boundaries (*16*). In this regard, nanoscale twins represent an optimal feature for structural metals (*9*). However, engineering these features into materials in a cost-efficient way is nontrivial. Traditionally, this can be achieved through either "bottom-up" methods, such as electrodeposition (*12*) and sputtering (*17*), or "top-down" methods, such as severe plastic deformation (*18*, *19*). However, almost all of these methods have been successfully accomplished in fcc metals (*20*, *21*), mostly in copper and steel (*19*, *22*), whereas generalization to hexagonal close packed (hcp) metals has been challenging. This challenge extends to a general method for creating a nanotwinned structure in a bulk sample without generating unfavorable residual stresses.

We demonstrate that hierarchical nanotwinned structures can be engineered in pure Ti (nominal composition in weight percentage: 99.95% Ti and 0.05% O) through massive mechanical twinning induced by means of a cryo-mechanical process. The ultralow O content (lower than commercial purity–grade Ti) is chosen to promote the twin propensity because O suppresses twinning in Ti (*23*). The cuboid-shaped specimens were repetitively forged along the three principal axes in liquid nitrogen (Fig. 1A) (*24*). The gentle uniaxial compression at each step controls the density of twins while preserving the initial grain structure of the material, which is in sharp contrast to other anisotropic processing methods such as extrusion and rolling, in which grains are elongated in one direction (*25*, *26*). The cryo-mechanically deformed materials were then heat treated (tempered) at an intermediate temperature (673 K) for 1 hour, which relieved the undesirable residual stress without triggering additional grain coarsening.

The electron backscattered diffraction (EBSD) map (Fig. 1B) reveals a complex multiscale twin structure in the multiaxis-forged Ti. The initial equiaxed grain structure is still visible, but after cryo-mechanical treatment, each grain contains profuse lenticular-shaped twins. These deformation features, introduced through a cryo-mechanical process, are retained during the subsequent heat treatment. Grain-boundary misorientation analysis suggests that these twins are mostly $\{10\bar{1}2\}$ tensile twins and $\{11\bar{2}2\}$ compression twins (fig. S1). A group of characteristic $\{10\bar{1}2\}$ nanotwins is captured in the transmission electron microscopy (TEM) micrograph (Fig. 1C), in which a twin boundary is highlighted in the high-resolution atomic lattice image (Fig. 1D). The nanotwins can often intersect with each other, leading to a complicated twin-twin network (fig. S2). Our TEM images show the same nanotwinned structure before and after 673 K tempering step (Fig. 1, E and F). After holding the sample at 673 K for 1 hour in the TEM, the nanotwinned structure is retained, but the strain contrast within the twins is diminished owing to residual stress-strain relaxation. We illustrate this strain relaxation using a quantitative representation from a nanobeam diffraction strain map computed before and after TEM in situ annealing (fig. S3). The statistical size distributions of these multiscale structures (Fig. 1G) show a macroscale matrix of randomly distributed, equiaxed grains in tens to hundreds of micrometers, a microscale twin skeleton with twin thickness in micrometers, and nanoscale twin networks with a twin thickness in tens to a couple of hundred nanometers.

The distinct multiscale twin structures result in substantially improved mechanical properties, which we characterized with uniaxial tensile tests at both room temperature (RT) and cryogenic (77 K) temperatures. We illustrate the true stress versus true strain response of the nanotwinned titanium and compare it with conventional coarse-grained Ti (with a grain size of ~100 μm) (Fig. 2A). At RT, the nanotwinned Ti exhibits a tensile strength of 500 MPa, with a tensile ductility (strain to failure) of ~70%. These values are improved by ~50 and ~17%, respectively, compared with the coarse-grained Ti. The yield strength of the as-processed material is controlled both by the reduced mean free path of dislocations in the local nanotwinned area, as well as the relatively coarser-grained matrix, rendering less of a Hall-Petch strengthening effect than nanocrystalline Ti (*27*) but a much higher work-hardening ability.

[1]Department of Materials Science and Engineering, University of California, Berkeley, CA 94720, USA. [2]National Center for Electron Microscopy, Molecular Foundry, Lawrence Berkeley National Laboratory, Berkeley, CA 94720, USA. [3]School of Materials Science and Engineering, Beihang University, Beijing 100191, China. [4]Materials Sciences Division, Lawrence Berkeley National Laboratory, Berkeley, CA 94720, USA.
***Corresponding author. Email: szhao@buaa.edu.cn (S.Z.); aminor@berkeley.edu (A.M.M.)**
†These authors contributed equally to this work.

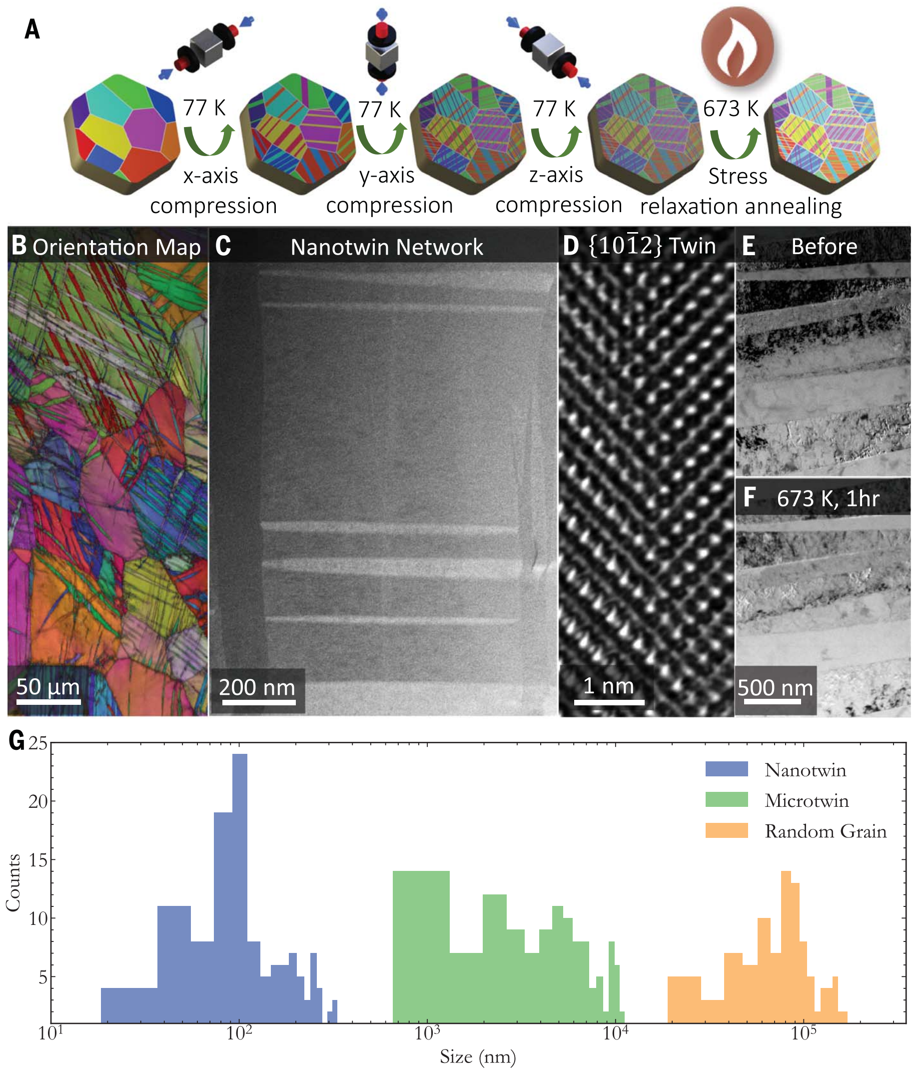

Fig. 1. Hierarchical microstructure of cryo-mechanically prepared nanotwinned Ti. (**A**) Schematic drawing of the cryo-mechanical process that results in the bulk nanotwinned Ti. (**B**) Orientation map showing the nanotwinned structure. (**C**) TEM micrograph of the nanotwin network. (**D**) Atomic-resolution image of a $\{10\bar{1}2\}$ twin boundary. (**E** and **F**) Images of (E) nanotwins at RT after cryo-mechanical process and (F) the same region after in situ TEM annealing at 673 K for 1 hour, showing the stability of the twinned structure and also the relaxation of strain fields from other internal defects. (**G**) Statistical size distribution of the hierarchical microstructure as determined with TEM (blue) and EBSD (green and yellow).

The mechanical properties of the nanotwinned Ti are further enhanced at 77 K, displaying a tensile strength of ~2 GPa and a tensile ductility of almost 100%. The combination of exceptional strength and ductility of nanotwinned Ti makes it superior to many Ti alloys and even certain cryogenic steels (fig. S4) (*28*–*30*). Different stages of plastic deformation can be qualitatively visualized from the plot of strain-hardening rate—the derivative of the flow stress with respect to strain, as a function of strain (Fig. 2B). The plot shows that the nanotwinned Ti displays better mechanical properties than those of its coarse-grained counterpart. This is manifested by a prolonged strain-hardening plateau at RT, which is followed by sizable resurgence in strain hardening at 77 K. Clearly, a sequential activation of deformation mechanisms is in evidence at different stages of plastic deformation. This evolution provides a steady, sustained source of hardening, which increases strength yet also effectively delays the necking, leading to an enhancement in ductility.

Focusing on the deformation mechanisms of the nanotwinned Ti at cryogenic temperatures, we characterized the deformation microstructures at different stages of plastic deformation by plotting the strain-hardening rate ($\theta = d\sigma/d\varepsilon$) normalized by the shear modulus (G), θ/G (Fig. 2C), as a function of the flow stress normalized by the yield stress [the Kocks-Mecking plot (*31*)] at 77 K and integrating it with the corresponding TEM observations. At the onset of plastic deformation, when the stress level is low (<~750 MPa), dislocation-mediated plasticity dominates, and a monotonic decrease in θ/G is expected. The corresponding microstructure (Fig. 2D) has dislocations confined within those prescribed twin boundaries. As the flow stress increases, twinning-induced plasticity takes over. At this stage, the nucleation and growth of primary and secondary twinning of different types evolve the twin-twin network into a more complicated multiscale hierarchy architecture, in which the twin spacing is reduced substantially into the nanoscale, leading to an enhanced dynamic Hall-Petch effect. A typical nanotwin network is shown in Fig. 2E. The increased dislocation density and the refined interspacing of the nanotwin network engender a higher activation stress for subsequent twinning, which in turn increases the flow stress (*32*). Macroscopically, this is manifested by an extended plateau followed by a rising strain-hardening rate. The strain-hardening rate drops rapidly toward the last stage of the plastic deformation, which is microstructurally associated with severe grain refinement, especially at the localization of deformation. The TEM micrograph (Fig. 2F) taken in the vicinity of the necking region shows a high density of equiaxial grains with a grain size of ~300 nm. Despite yielding a high flow stress, these ultrafine grains make both dislocation activity and twinning (*33*) difficult to operate and consequently jeopardize the strain-hardening ability. We also analyzed the microstructure in the as-fractured sample (fig. S5) and observed that the necking region displays a much finer microstructure with a sharper $\{0001\}\langle 10\bar{1}0\rangle$ texture component than in regions further away, which is consistent with the TEM observations (Fig. 2F).

Dimensional refinement has long been known to enhance strength and ductility at low temperatures (*29*). The difference here is that the structure evolves during deformation into an optimal hierarchical structure defined by the coarse grains, twin-twin skeleton, nanotwins, and ultrafine grain refinement. In addition to these strengthening mechanisms, the distinct nanotwin architecture plays an effective toughening role in retarding crack extension (*34*). We show that an advancing crack is deflected on a route across the nanotwin barrier (Fig. 2G). Further evidence that nanotwins can either deflect or block crack propagation is shown in fig. S6; the growth of microcracks was observed during in situ TEM tensile testing at RT. This implies that our nanotwinned Ti may display enhanced damage tolerance.

Among all the mechanisms described above, twinning-induced plasticity plays the pivotal role. Using quasi in situ EBSD characterizations, we were able to capture this evolution

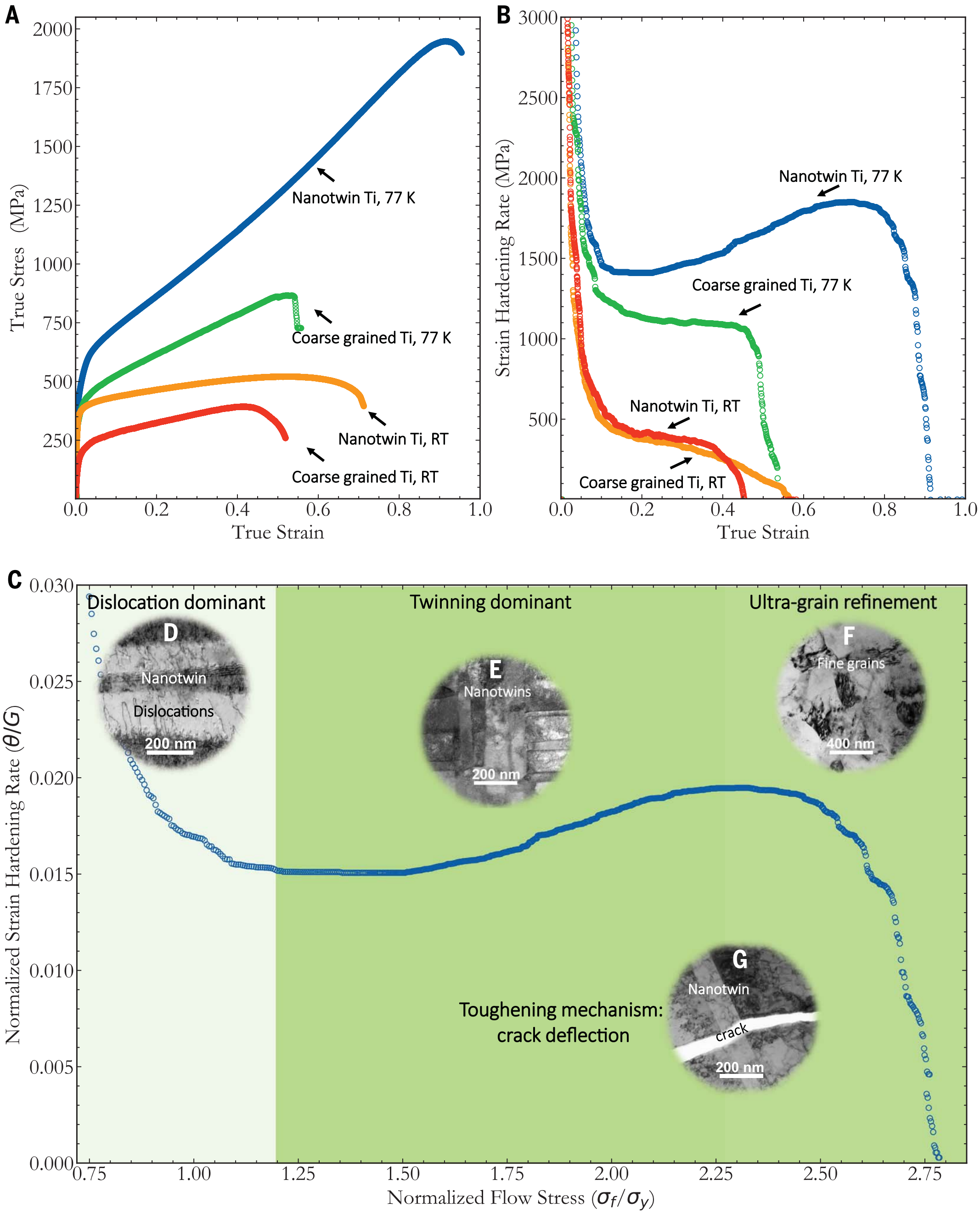

Fig. 2. Mechanical characterization of the hierarchical nanostructured Ti. (**A**) True stress versus true strain curves with a nominal strain rate of 10^{-3} s^{-1} and the comparison with its coarse-grained counterpart. (**B**) Corresponding plots of strain-hardening rate versus true strain. (**C**) The stages of plastic deformation at 77 K are shown schematically along with a plot of the strain-hardening rate normalized by the shear modulus, $\theta/G = (d\sigma/d\varepsilon)/G$, as a function of the flow stress normalized by the yield stress. The normalized strain-hardening rate versus normalized flow stress curve clearly shows that there are multiple stages of plastic deformation. (Insets) The characteristic deformation features at the different stages.

of twinning, detwinning, and retwinning. We collected a series of EBSD analyses of the same region with incremental degrees of plastic strain at 77 K (Fig. 3). We also collected orientation maps (Fig. 3, A to F) and the corresponding boundary misorientation maps (Fig. 3, G to L). We show the initial twin structure in Fig. 3A. Correspondingly, we can identify two types of twins with distinctive misorientations by the boundary misorientation map (Fig. 3G): $\{10\bar{1}2\}$ tensile twins with a misorientation angle of 85° (orange) and $\{11\bar{1}2\}$ compression twins with a misorientation angle of 65° (green). After 5% plastic strain, multiple $\{11\bar{2}2\}$ twins are nucleated at grain boundaries (Fig. 3, B and H) and grow with further deformation [engineering strain (ε) = 10%] (Fig. 3, C and I) until secondary $\{10\bar{1}2\}$ twins start to nucleate at the primary $\{11\bar{2}2\}$ twin boundaries (ε = 15%) (Fig. 3, D and G). Subsequently, these secondary $\{10\bar{1}2\}$ twins interact with the previously developed primary $\{11\bar{2}2\}$ twins, propagate (ε = 25%) (Fig. 3, E and K), and eventually consume the original grain structure (ε = 35%) (Fig. 3, F and L). Above 25% plastic deformation, the twin-twin interactions produce profuse "junctions" of fine grains within the original coarse grains. We summarized the length fractions of each type of twin and the total twin boundaries in Fig. 3M. After a rapid growth rate of the total twin fraction, the combination and competition of continuous twinning and detwinning caused a much-reduced growth rate of the twin fraction at the microscale. However, even when the microscale twin fraction saturates (~70%), the nanotwin density seems to keep increasing until severe twin-twin intersections and twin-boundary rotations come into play toward the end of plastic deformation, which is evident in the TEM observations (Fig. 2C). Despite the complex twin-structure evolution, the flow stress increases

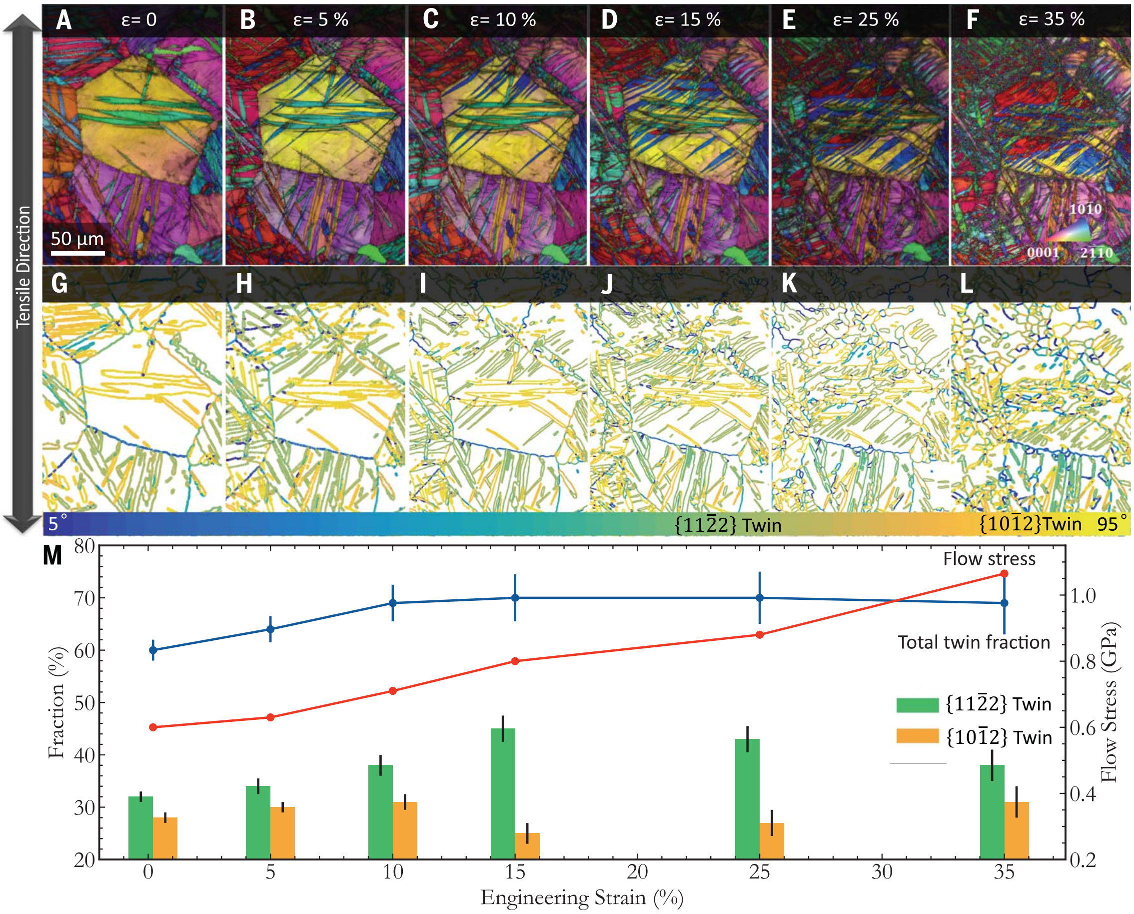

Fig. 3. Microstructure evolution of nanotwinned Ti. (**A** to **F**) Orientation maps (overlaid with image quality) captured in an area of interest at progressive strain levels of up to 35% engineering strain. (**G** to **L**) The corresponding grain boundary misorientation maps show the evolution of the two characteristic twin boundaries: $\{11\bar{2}2\}$ compression twins with a misorientation of ~65° (green), and $\{10\bar{1}2\}$ tensile twins with a misorientation of 85° (orange-yellow). Twins, which nucleate at either random grain boundaries or preexisting twin boundaries, will propagate, grow, and intersect with each other. Toward higher strains, twin-twin intersections form junctions of fine grains within the original coarse grains. (**M**) Evolution of the length fraction of the $\{11\bar{2}2\}$ and $\{10\bar{1}2\}$ twin boundaries as well as the fraction of the total twin boundaries, which increases initially and saturates at about 15% engineering strain. The full EBSD scans contain a much larger area with many more grains. For display purpose, only a fraction of the data was shown in (A) to (L). The statistics of twins in (M), however, are measured from the full datasets.

monotonically as a function of strain. We can attribute this to (i) the fraction of nanotwins still increasing beyond what can be resolved with the quasi–in situ EBSD analysis and (ii) the twin-twin junctions within the grains refining the grain size even further to produce more interfaces that impede dislocation motion (*19*). Nevertheless, both mechanisms lead to a dynamic Hall-Petch effect (*27*, *35*, *36*): mobile dislocations confined by relative rigid interfaces, which renders a higher resistance to plastic deformation. We show evidence for this (fig. S7), in which a group of mobile $\langle a \rangle$ type screw dislocations are "arrested" by two nanotwins. Moreover, the activation of twinning mode depends mostly on the maximum Schmid factor criterion (fig. S8). Such a marked microstructural evolution is also accompanied by the development of $\{0001\}\ \langle 10\bar{1}0\rangle$ texture (fig. S9). Such texture is not only caused by the twinning but also by $\langle a \rangle$ type dislocation slip on the $\{10\bar{1}0\}$ prismatic planes (*37*, *38*).

Nanocrystalline metals become progressively unstable at elevated temperatures because the profuse interfaces can be consumed by grain growth, through Ostwald ripening (*16*). Therefore, the temperature that marks the onset of grain coarsening, which is usually proportional to the melting point of the material, eventually limits the useful service temperature of such nanocrystalline metals. Ti has a reasonably high melting temperature (1941 K) among structural metals, and the usefulness of the nanotwinned structure is dependent on its thermal stability. In situ TEM heating experiments revealed that the nanotwin structure is thermally stable up to 873 K (Fig. 4, A and B). Further heating, however, led to aggressive oxidation (Fig. 4, C and D) because the sample was a thin electron-transparent foil, and the microscope was only under a nominal vacuum of roughly 1.3×10^{-3} Pa (~10^{-5} torr). At around 1123 K (Fig. 4E), severe oxidation started to develop (white dotted islands), yet the nanotwin network remained relatively preserved. These in situ TEM heating experiments were further corroborated by means of ex situ annealing and post mortem EBSD analysis; we show that heating of the nanotwinned Ti at 673 K for 48 hours does not result in either noticeable grain growth or an obvious reduction in the number of twin boundaries (Fig. 4, F and G). The local kernel averaged misorientation maps (Fig. 4, H and I) suggest that the annealed sample (Fig. 4I) has relatively lower misorientation within grains, inferring that the density of geometrically necessary dislocations is reduced. The good thermal stability of the nanotwinned Ti enables the preservation of the hierarchical microstructure at elevated temperatures, indicating that the material has the capacity to operate over a wide temperature range, covering the majority of traditional applications of Ti-based alloys.

Tensile tests were also conducted at elevated temperatures of up to 873 K (600°C). The yield strength decreases monotonically as a function of temperature (Fig. 4E), in both coarse-grained and nanotwinned Ti. At these low stress levels, deformation twinning is progressively difficult and eventually ceases to occur, rendering dislocations as the primary carrier of plasticity. Even so, the strength of the nanotwinned Ti is still much higher than its coarse-grained counterpart at all the temperatures studied.

By creating a synergy of deformation mechanisms—most notably, deformation

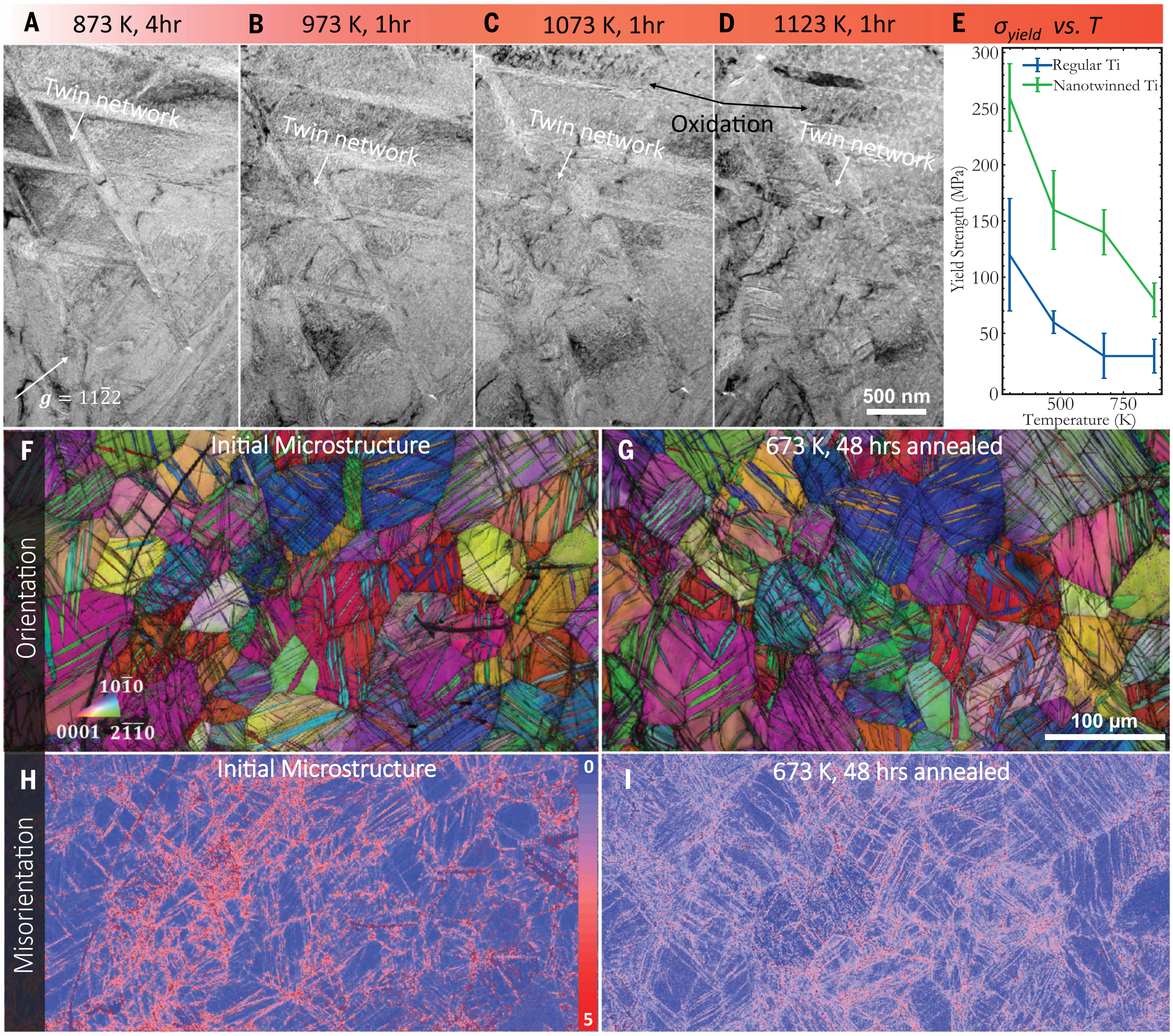

Fig. 4. Thermal stability of the nanotwinned Ti. (**A**) In situ TEM heating experiments show that the nanotwin network (white arrows) is thermally stable up to 600°C (873 K). (**B** and **C**) Above 700°C (973 K), the contrast of the twin interface is getting progressively weaker. (**D**) At around 850°C, oxide flakes start to show up in the matrix. (**E**) Yield strength of the nanotwinned Ti as a function of temperature and the comparison with the coarse-grained materials. (**F**) EBSD IPF mapping and (**H**) the corresponding kernel averaged misorientation (KAM) mapping of the as fabricated nanotwinned titanium. (**G**) IPF and (**I**) KAM maps of the same sample (in similar regions of interest) annealed at 400°C for 48 hours.

twinning—fcc materials, especially CrCoNi-based high-entropy alloys, can be developed with remarkable combinations of strength and ductility that are further enhanced at cryogenic temperature (*39*, *40*). In this work, by using cryo-mechanical processing, we have achieved this in a hcp material, Ti, without the need for any alloying elements.

We have introduced a straightforward and efficient method to produce thermally stable, bulk nanotwinned Ti. The mechanical properties of this material, specifically its strength and tensile ductility, are enhanced to a large extent from ambient to cryogenic temperatures. The introduction of a multiscale twin architecture effectively subdivides the original grains and substantially refines the mean free path of dislocations. Subsequently, the tensile and compressive twins induced during multi-axis–forging can continue to twin, detwin, and retwin, which leads to an enhanced work-hardening ability. Accordingly, nonuniform plastic flow is postponed. This combination of properties suggests that such nanotwinned Ti could be applied to a wide range of applications, especially those involving extreme temperatures.

What sets the nanotwin Ti apart from many other Ti alloys is its cryogenic performance, with attractive strength as well as ductility that is better than even the high-strength Ti-6Al-4V alloy (*41*). This suggests that nanotwin Ti is a strong candidate for cryogenic applications. Some examples include the retaining rings of superconducting magnets, structural parts of the liquefied natural gas storage tanks, and materials exposed to deep ocean and deep space environments. Historically, these are applications for cryogenic steels such as austenitic 18Mn-5Cr (*30*) and 32Mn-7Cr-0.6Mo-0.3N alloys (*42*) and ferritic Fe-9Ni alloy (*29*). Nanotwin Ti outperforms these materials in both strength and ductility (fig. S4), at half the density.

The enhanced work-hardening ability due to massive twinning at liquid-nitrogen temperature indicates that nanotwinned Ti may display a high impact resistance at higher strain rates (*43*) because twinning in hcp metals is also promoted by reducing the time scale of deformation (*44*). Nanotwinned Ti may also possess sound radiation-damage tolerance because the profuse nanotwin boundaries provide a high density of interfaces to channel point defects and therefore prevent the formation of voids (*45*, *46*). In addition, the thermal stability of nanotwinned Ti renders it applicable at temperatures as high as 873 K, which is comparable with many industrial power plant applications, and at the lower-temperature regions in gas-turbine engines. Moreover, compared with the heavily alloyed, highly expensive high-entropy alloys (*39*, *40*, *47*) with similar mechanical properties, no alloying elements are involved in the nanotwin Ti. This makes it a "simpler" alloy that is economically attractive and easily recyclable (*2*). All of these beneficial factors make nanotwinned Ti not only scientifically interesting but also a potential industrial product.

REFERENCES AND NOTES

1. G. Lütjering, J. C. Williams, *Titanium: Engineering Materials and Processes* (Springer, ed. 2, 2007).
2. X. Li, K. Lu, *Science* **364**, 733–734 (2019).
3. X. Wu *et al*., *Proc. Natl. Acad. Sci. U.S.A.* **112**, 14501–14505 (2015).
4. S. Yip, *Nature* **391**, 532–533 (1998).
5. M. A. Meyers, A. Mishra, D. J. Benson, *Prog. Mater. Sci.* **51**, 427–556 (2006).
6. K. S. Kumar, H. Van Swygenhoven, S. Suresh, *Acta Materialia* **51**, 5743–5774 (2003).
7. R. Z. Valiev, I. V. Alexandrov, Y. T. Zhu, T. C. Lowe, *J. Mater. Res.* **17**, 5–8 (2002).
8. K. Lu, L. Lu, S. Suresh, *Science* **324**, 349–352 (2009).
9. L. Lu, X. Chen, X. Huang, K. Lu, *Science* **323**, 607–610 (2009).
10. Q. Huang *et al*., *Nature* **510**, 250–253 (2014).
11. Z. Zhang *et al*., *Nat. Commun.* **8**, 14390 (2017).
12. L. Lu, M. L. Sui, K. Lu, *Science* **287**, 1463–1466 (2000).
13. E. Ma *et al*., *Appl. Phys. Lett.* **85**, 4932–4934 (2004).
14. Z. Cheng, H. Zhou, Q. Lu, H. Gao, L. Lu, *Science* **362**, eaau1925 (2018).
15. Q. Pan, H. Zhou, Q. Lu, H. Gao, L. Lu, *Nature* **551**, 214–217 (2017).
16. G. Gottstein, L. S. Shvindlerman, *Grain Boundary Migration in Metals: Thermodynamics, Kinetics, Applications* (CRC Press, 1999).
17. A. M. Hodge, Y. M. Wang, T. W. Barbee Jr., *Scr. Mater.* **59**, 163–166 (2008).
18. R. Valiev, *Nat. Mater.* **3**, 511–516 (2004).
19. Y. Wei *et al*., *Nat. Commun.* **5**, 3580 (2014).
20. L. Sun, X. He, J. Lu, *npj Computational Materials* **4**, 6 (2018).
21. X. Li, L. Lu, J. Li, X. Zhang, H. Gao, *Nat. Rev. Mater.* **5**, 706–723 (2020).
22. F. K. Yan, G. Z. Liu, N. R. Tao, K. Lu, *Acta Mater.* **60**, 1059–1071 (2012).
23. H. Conrad, *Prog. Mater. Sci.* **26**, 123–403 (1981).
24. Materials and methods are available as supplementary materials.
25. S. W. Choi, J. W. Won, S. Lee, J. K. Hong, Y. S. Choi, *Mater. Sci. Eng. A* **738**, 75–80 (2018).
26. J. W. Won *et al*., *Scr. Mater.* **178**, 94–98 (2020).
27. Z. C. Cordero, B. E. Knight, C. A. Schuh, *Int. Mater. Rev.* **61**, 495–512 (2016).
28. K. A. Yushchenko, in *Advances in Cryogenic Engineering Materials*, A. F. Clark, Ed. (Springer, 1984), pp. 271–282.
29. C. K. Syn, S. Jin, J. W. Morris, *Metall. Trans., A, Phys. Metall. Mater. Sci.* **7**, 1827–1832 (1976).
30. R. Miura, K. Ohnishi, H. Nakajima, Y. Takahashi, K. Yoshida, in *Austenitic Steels at Low Temperatures* (Plenum Press, 1983), pp. 287–293.
31. H. Mecking, U. F. Kocks, *Acta Metall.* **29**, 1865–1875 (1981).
32. Y. T. Zhu, X. Z. Liao, X. L. Wu, *Prog. Mater. Sci.* **57**, 1–62 (2012).
33. J. L. Sun *et al*., *Scr. Mater.* **69**, 428–431 (2013).
34. Z. Zeng, X. Li, L. Lu, T. Zhu, *Acta Mater.* **98**, 313–317 (2015).
35. N. Hansen, *Scr. Mater.* **51**, 801–806 (2004).
36. F. Otto *et al*., *Acta Mater.* **61**, 5743–5755 (2013).
37. C. N. Tomé, R. A. Lebensohn, U. F. Kocks, *Acta Metall. Mater.* **39**, 2667–2680 (1991).
38. D. N. Williams, D. S. Eppelsheimer, *Nature* **170**, 146–147 (1952).
39. B. Gludovatz *et al*., *Science* **345**, 1153–1158 (2014).
40. B. Gludovatz *et al*., *Nat. Commun.* **7**, 10602 (2016).
41. K. Nagai *et al*., *ISIJ Int.* **31**, 882–889 (1991).
42. F. Ruidong, Z. Yangzeng, R. Yibin, *J. Mater. Eng. Perform.* **10**, 456–459 (2001).
43. D. R. Chichili, K. T. Ramesh, K. J. Hemker, *Acta Mater.* **46**, 1025–1043 (1998).
44. S. G. Song, G. T. Gray, *Metall. Mater. Trans., A Phys. Metall. Mater. Sci.* **26**, 2665–2675 (1995).
45. Y. Chen *et al*., *Nat. Commun.* **6**, 7036 (2015).
46. R. W. Grimes, R. J. M. Konings, L. Edwards, *Nat. Mater.* **7**, 683–685 (2008).
47. Z. Li, K. G. Pradeep, Y. Deng, D. Raabe, C. C. Tasan, *Nature* **534**, 227–230 (2016).

ACKNOWLEDGMENTS

Funding: The authors gratefully acknowledge funding from the US Office of Naval Research under grants N00014-17-1-2283 and N00014-19-1-2376. Q.Y. and R.O.R. also acknowledge the support from the US Department of Energy, Office of Science, Basic Energy Sciences, Materials Sciences and Engineering Division under contract DE-AC02-05-CH11231 to the Damage-Tolerance in Structural Materials Program (KC13) at the Lawrence Berkeley National Laboratory (LBNL). Work at the Molecular Foundry was supported by the Office of Science, Office of Basic Energy Sciences, of the US Department of Energy under contract DE-AC02-05CH11231. The authors thank Timet for providing the high purity titanium and also acknowledge helpful discussions with D. Chrzan, M. Asta, and J. W. Morris Jr.. **Author contributions:** S.Z. formulated the original ideas, which were approved by A.M.M; S.Z., R.Z, and Q.Y. conducted the tensile tests, and R.Z. performed the digital image correlation analysis to calibrate the strain. S.Z. and Q.Y. performed EBSD experiments and analyzed the data. Q.Y. and J.E. conducted mechanical testing at elevated temperatures. S.Z. performed conventional scanning TEM (STEM), TEM, and high-resolution TEM characterization as well as 4D-STEM experiments. R.Z. and S.Z. conducted the in situ TEM heating experiments. S.Z., R.O.R., and A.M.M. drafted the manuscript, and all the authors contributed to the discussions. R.O.R and A.M.M. supervised the project. **Competing interests:** The authors declare no competing interests, financial or otherwise. Readers are welcome to comment on the online version of the paper. **Data and materials availability:** The data that support the findings of this study are available at an online data repository: https://figshare.com/projects/Cryoforged_nanotwinned_titanium_with_ultrahigh_strength_and_ductility/119352. Correspondence and requests for materials should be addressed szhao@buaa.edu.cn (S.Z.) and aminor@berkeley.edu (A.M.M.).

SUPPLEMENTARY MATERIALS

https://science.org/doi/10.1126/science.abe7252
Materials and Methods
Supplementary Text
Figs. S1 to S16
References (*48*–*58*)
Movies S1 to S3

10 September 2020; resubmitted 25 March 2021
Accepted 4 August 2021
10.1126/science.abe7252

Science

Cryoforged nanotwinned titanium with ultrahigh strength and ductility

Shiteng ZhaoRuopeng ZhangQin YuJon EllRobert O. RitchieAndrew M. Minor

Science, 373 (6561), • DOI: 10.1126/science.abe7252

Titanium gets some twins

Introducing a network of nanotwins is known to improve the properties of face-centered cubic metal alloys. Zhao *et al*. used gentle compression in liquid nitrogen to introduce a similar network of nanotwins in hexagonal closed-packed titanium. By starting with a titanium that has little oxygen, the twin network can be more easily established. The nanotwinned network improved the yield strength by 50% and ductility by 20% at room temperature. The cryogenic properties were even better, with a yield strength of two gigapascals and a tensile ductility of 100% before failure. —BG

Science (ISSN) is published by the American Association for the Advancement of Science. 1200 New York Avenue NW, Washington, DC 20005. The title *Science* is a registered trademark of AAAS.